Universiteit Antwerpen

This item is the archived peer-reviewed author-version of:

CO_2, CH_4 and N_2 separation with a 3DFD-printed ZSM-5 monolith

Reference:
Couck Sarah, Lefevere Jasper, Mullens Steven, Protasova Lidia, Meynen Vera, Desmet Gert, Baron Gino V., Denayer Joeri F. M..- CO_2, CH_4 and N_2 separation w ith a 3DFD-printed ZSM-5 monolith
Chemical engineering journal - ISSN 1385-8947 - 308(2017), p. 719-726
Full text (Publisher's DOI): https://doi.org/10.1016/J.CEJ.2016.09.046
To cite this reference: http://hdl.handle.net/10067/1356220151162165141

uantwerpen.be
Institutional repository IRUA

CO_2 adsorption with a 3DFD-printed ZSM-5 monolith

Sarah Couck[1], Jasper Lefevere[2,3], Steven Mullens[3], Lidia Protasova[3], Vera Meynen[2,3], Gert Desmet[1], Gino V. Baron[1], Joeri F.M Denayer[1,*].

1. Chemical Engineering department, Vrije Universiteit Brussel, Pleinlaan 2, 1050 Brussel, Belgium

2. Laboratory of Adsorption and Catalysis, University of Antwerp, Universiteitsplein 1, 2610 Wilrijk, Belgium

3. Vlaams Instituut voor Technologische Ontwikkeling (VITO NV), Boeretang 200, 2400 Mol, Belgium

* joeri.denayer@vub.ac.be / +32 2 629 1798

Abstract

A new method for producing zeolitic monoliths is used to produce a ZSM-5 based monolith for gas separation. The new method involves the 3DFD (Three Dimensional Fiber Deposition) printing of several layers of zeolite fibers on top of each other in a well-defined way, resulting in an open monolithic structure with open and inter-connected channels. The monolithic structure, consisting of ZSM-5 zeolite, was characterized with SEM, Ar and Hg porosimetry. Single component isotherms of CO_2, CH_4 and N_2 were recorded on the 3DFD-printed ZSM-5 monolith, at different temperatures (283K, 291K, 302K and 309K) using a gravimetric method. Isosteric heats of adsorption show that CO_2 is the most strongly adsorbing component, in order followed by CH_4 and N_2. The monolithic structure was subjected to breakthrough separation experiments with CO_2/N_2 and CO_2/CH_4 gas mixtures. Excellent separation performance is achieved. Moreover, the ZSM-5 monolith can be easily regenerated in isothermal conditions.

Keywords: adsorption, separation, CO_2, 3D-printing, monolith, ZSM-5

Highlights:

- Three-dimensional fiber printing of ZSM-5 zeolite as self-standing monolith
- Adsorption properties of CO_2, N_2 and CH_4 on the 3D printed ZSM-5 monolith
- Good CO_2 separation performance with this 3D printed ZSM-5 monolith

Introduction

Most adsorbents are produced as porous, micron-sized powder materials and are thus not suitable to be directly used in adsorption processes. In order to avoid excessive pressure drop during flow of gas or liquid streams through a packed bed of adsorbent, these powders are shaped into larger particles or structured adsorbents. Extrudates, beads or pellets with a size of several millimeters are widely used in industrial processes. An important development with respect to the production of such particles is the production of binderless zeolite-based materials, with a significantly larger adsorption capacity as a result of the larger amount of active material on a volumetric basis [1-3]. The most important disadvantages of pellets, beads and extrudates include the relatively large pressure drop they generate at high flow rates and the presence of mass transfer limitations as a result of slow diffusion of molecules to the core of the particles. A trade-off between these two effects limits the possibilities to optimize packed bed adsorptive separation processes; e.g. decreasing pellet size allows to reduce mass transfer limitations but this in turn leads to larger pressure drops. In practice, bed geometry (length/width of the packed bed) is adapted to limit pressure drop [4-6]. Nevertheless, classical packed beds are not ideal for processes in which very short cycle times or very high gas or liquid velocities are required.

Other types of adsorbent formulation that allow eliminating the limitations mentioned above are thus of large interest. Monolithic adsorbents are superior to classical packed bed adsorbents in terms of pressure drop and mass transfer kinetics. The honeycomb structure, mostly known from catalytic exhaust treatment in the automotive industry, is a well-known example, but monolithic structures are also used in liquid chromatography and heterogeneous catalysis [7-10].

These so-called honeycomb monoliths are materials with parallel gas flow channels, which can have various dimensions and shapes. Numerous scientific papers and reviews discuss the potential advantages of monolithic structures; low pressure drop at high flow rates, uniform flow distribution and improved mass-transfer are a few that are mentioned [5, 6, 11-14]. With respect to the active phase, two major types of monolithic structures can be distinguished. In the first type, the monolithic structure consists of an inert support structure like alumina-based ceramics (e.g. cordierite), carbon-based materials or metallic structures. The active phase needed for the catalytic or adsorptive process, for example a zeolite, is then coated on the monolithic structure by means of wash-coating, impregnation or in-situ crystal growth [4, 6, 11, 12]. In the second type, the monolithic structure itself already consists of the active phase, i.e. the so-called self-standing monolith. To produce such a bulk zeolite monolith and provide its required mechanical strength, the zeolite powder is mixed with a binder material. The resulting paste is then molded into the desired configuration by means of extrusion [4, 11, 13-15]. In recent developments, the presence of a binder is omitted by converting the binder material into the active phase. Jänchen et al. produced a monolith consisting of zeolite 4A and kaolin as an intermediate binder, where the kaolin is later converted into zeolite 4A, resulting in a binderless monolith[1]. Not only zeolites are used to prepare such monolithic structures, also carbon is regularly used in monolithic structures [16-18].

Although monolithic structures have been intensively studied and used over the past decades, mainly in the field of car exhaust catalyst systems, much less studies are devoted to adsorption or adsorptive separation. Ribeiro *et al.* studied a commercial available carbon honeycomb monolith for adsorption equilibria and kinetics of pure CO_2, CH_4, and N_2. This fundamental data can be further used in simulations and modeling of adsorption processes

such as PSA [17]. Rezaei *et al*. and Mosca *et al.* developed a NaX coated cordierite monoliths by growing a zeolite film on the cordierite support for PSA or VSA applications. They studied breakthrough profiles of CO_2 in different monoliths and compared them to packed bed columns [6, 12]. Rezaei *et al.* concluded that the structured adsorbents show less effect of pressure drop when looking at shorter cycle times and thus leading to better performance. When longer cycle times are considered, it are the beads that show better performance. Grande *et al.* prepared and investigated an extrudated 4A monolith (with methyl cellulose and methyl siloxane ether as binders) for adsorption of propane and propylene. They report experimental as well as modeling data. Adsorption equilibrium was comparable to commercial extrudates, diffusivity coefficients were however three times lower as compared to the commercial ones, which is attributed to partial micropore blocking. A mathematical model for adsorption of streams was developed and validated with breakthrough data [14]. Hasan *et al.* prepared a self-standing 5A monolith by creating parallel channels, by means of a channeling tool with pins, in a monolithic body. This structure was subjected to breakthrough measurements of CO_2 in presence of N_2. It was found that the monolithic structure surpassed a classical column packed with pellets due to faster diffusivity and lower pressure drop while having a comparable capacity [13]. Recently, an extruded monolithic structure containing MIL-101, a Metal-Organic Framework, was prepared by the paste extrusion technique. The MIL-101 monolith was characterized with XRD, SEM, mercury intrusion, single component isotherms and breakthrough experiments. The authors demonstrated that the structure could be regenerated under mild conditions and that it showed excellent adsorption of CO_2 [19]. Theoretical work of Razaei and Webley report a methodology to examine the performance of different adsorbent configurations based on a variety of analytical and numerical models [20]. They came to the conclusion that monoliths

can be proper candidates if appropriate high cell densities and low voidages are used. Low density monoliths lead to lower mass and surface area based on volumetric units that diminishes the overall rate constant in the monoliths as compared to packed beds [20].

A survey of literature shows that the largest part of academic studies has been conducted on commercially available monoliths. Since the extrusion process, which is used to produce monoliths, is not easy to perform on lab scale, most researches have to rely on existing monolithic structures. Only few authors synthesized the monolithic materials themselves. With the advent of 3D-printing techniques [21-25], new possibilities in the synthesis of structured emerge.

In this work, we describe a 3DFD (Three Dimensional Fiber Deposition) printing method to produce self-standing monolithic structures [24, 25] with a high potential for sorption and separation processes. This method allows the precise fabrication of monolithic structures, with large control on channel size, fiber thickness and geometry of the channels. Traditional extrusion methods generate monoliths with parallel channels that are not connected to each other. In the method presented here, zeolite containing fibers are printed in a layer-wise manner, in which the distance between the fibers, their thickness and orientation to each other in subsequent layers can be controlled. As a result, an interwoven structure with highly adaptable architecture and interconnected channels (radial porosity) is obtained. This approach allows for very specific design of the monolithic structure.

In this contribution, a monolithic structure containing ZSM-5 zeolite is produced and tested for CO_2 adsorption and separation from N_2 and CH_4 by means of isotherm measurements and breakthrough experiments.

Materials and Methods

3DFD-printing of the ZSM-5 monolith

ZSM-5 powder (Si:Al = 25, d_{50} = 8µm, provided by Süd-chemie) was mixed with a watery binder suspension containing colloidal silica (Ludox HS-40, Sigma-Aldrich) and milled bentonite (VWR, d_{50}= < 10µm). The composition of this mixture consist of 65 wt% ZSM-5 zeolite and 35 wt% of binder (binder = 50wt% bentonite and 50wt% ludox). A binary binder system was used as this yielded monoliths with improved mechanical strength as compared to a single binder system. The use of bentonite allowed for an easy writing of the structures without any defects, while silica on the other hand assisted in binding the zeolite and bentonite particles together. The zeolite and suspension are mixed using a planetary centrifugal mixer for 2 minutes at 1900 rpm. This paste is fed to the reservoir of a computer numerical controlled machine (CNC), containing a nozzle to extrudate the paste (diameter of 900 µm or 400 µm). By means of continuous extrusion of fibers and the well-programmed movement of the CNC machine, a well-defined structure was build up layer by layer (fibers perpendicular to each other in this case) (see Figure 1). The structure was printed at a temperature of 293K and a relative humidity of 80%; porosity between fibers was programmed to be 68%. When printing was completed, the structures are left to dry in a controlled atmosphere (293K and 80% RH). Drying under controlled atmosphere was done to allow slow condensation and drying of the structure in order to prevent defects and cracks induced by shrinkage and strain upon fast loss of water from the structure. Subsequently a calcination process was applied (1K/min, 823K for three hours). An XRD pattern of the 3DFD printed monolith is shown in the supporting information (Figure S7). From this XRD pattern, it is clear that the printed ZSM-5/binder mixture retained its crystalline nature.

Characterization and isotherm measurements Ar porosimetry was carried out with an Autosorb AS-1 from Quantachrome to determine the surface area and pore volume[26, 27]. The surface area was calculated with the BET method and the pore volume was determined via the DFT method. Hg porosimetry was performed with two Thermo-Finnigan porosimeters (Pascal 140 for the range 4-100 μm diameter and Porosimeter 2000 for the range 0.008-15 μm diameter). Measurement starts at vacuum up to 2 bar, followed by measurement from 1 to 2000 bar. Scanning electron microscopy was performed using a Jeol JSM-6400. Single component gravimetric isotherms of N_2, CH_4 and CO_2 on powder and monolithic structure were recorded using a gas dosing system and a magnetic suspension balance from Rubotherm GmbH. Prior to these measurements, the material was activated at 573K, between measurements a regeneration under vacuum and a temperature elevation till 373K was conducted.

Separation experiments Breakthrough experiments were carried out with an in-house built system. A detailed description of this setup can be found in earlier work [28]. Calculation of the amount adsorbed is based on the formula given by Sunil *et al.* [29]. Monolithic structures were given the shape of a cylinder with a diameter of around 2.1 cm. To obtain a reasonable column length, several cylinders of 2.1 cm were stacked and wrapped with Teflon tape to eliminate the escape of gas at the sides. This created a continuous monolithic column with a length of 10.5 cm. The Teflon wrapped cylinder was inserted in a metal holder column and placed inside an oven. In most of the experiments, the total flow rate through the column was 200 Nml/min, whereof 150 Nml/min was a Helium dilution flow, the remaining 50

Nml/min consisted of the CO_2-N_2 or CO_2-CH_4 mixture. Composition of the mixtures varies from 10 mole% CO_2, to 25 mole%, 50 mole% and finally 75 mole% CO_2 in combination with both N_2 or CH_4.

Results and discussion

Figure 1 (A and B) shows a picture of two monolith units with different fiber diameter (900µm and 400µm) and inter fiber distance (1100 µm and 500 µm respectively), with a diameter of about 2.1 cm and a height of 2.5 cm. SEM pictures of the monolithic structure with 400 µm fibers are shown in Figure 1 on the right side. This figure shows the build-up of the monolithic structure from the top- and side view. The fibers in these structures were printed in a 1-1 direction, such that the fibers of each row are perpendicular to the next row of fibers. This fiber printing pattern results in a structure with straight channels. The fibers used to fabricate this structure consist of 65 wt% ZSM-5 zeolite and 35 wt% of binder (50wt% bentonite with 50wt% ludox HS-40). As can be perceived from the side view of the monolith (Figure 1, right side), the channels between the fibres are interconnected. As a result, the gas flow is not restricted to the same channel but can flow from one to the other channel.

Argon porosimetry was performed on both the parent ZSM-5 powder as on the monolithic structure to determine surface area and pore volume (see Table 1). Argon isotherms are plotted in Figure 2 (left). The presence of the binder in the monolithic structure results in a decrease in BET-surface area, from 414 m^2/g for the powder to 305 m^2/g or 261 m^2/g for the 400 µm and 900 µm monolith respectively. Also the micropore volume decreases from 0.15 cc/g to 0.10 or 0.11 cc/g (depending on monolith), which corresponds to a relative decrease of 27% as average, which is somewhat lower than the amount of binder used to produce the monolithic material. This decrease in micropore volume is also clearly visible in the lower adsorption branch of the monoliths as compared to the powder. Nevertheless, mesopore volume on the other hand is higher for the monolith as it has a large fraction of mesopores between the crystals, as can be perceived from the pore size distribution in Figure 3. From

Hg porosimetry measurements (see Figure 2, right) the larger pores in the monolith can be measured. The larger, printed run-through channels are however not visible as they are already filled up with Hg before the start of the measurement. During the low pressure measurement Hg essentially filled the dilatometer and no useful pore size distribution could be extracted. At the high pressure measurement, for both monoliths, a peak in pore size distribution is visible between 1 and 3 µm (see Figure 3, right). These values correspond with the pores formed between crystals in the monolith. Pores of the same inter-crystalline pore sizes can be distinguished on the SEM pictures (Figure 1,D). Mesopores of about 11 nm are clearly visible for the monolith with 400 µm fibers, while for the 900µm fibers these mesopores are less present. As these mesopores are not found in Ar porosimetry it is possible that at those high Hg pressures, the material starts to deform and the monolith with the smaller fibers is likely to be more susceptible to deformation that the monolith with larger fibers. In order to determine the large pores of the channels, a piece with known geometry of the monoliths was inserted in a calibrated flask and water was added to fill up the flask. The amount of water needed is then compared to the amount of water needed to fill up an empty flask. Void volume as calculated from this method is also found in Table 1. The corresponding porosity is calculated to be 74 and 77 % for the 400 µm and 900 µm monolith respectively, which is somewhat higher than the programmed 68% for the printing of the zeolite paste. Deviation can be attributed to adsorption of water or the uptake in the intercrystalline space by capillarity.

To characterize the gas adsorption properties of the 3DFD-printed ZSM-5 monolith (400 µm fiber monolith), single component isotherms of N_2, CH_4 and CO_2 were recorded and compared to the ZSM-5 zeolite in powder form at a temperature of 302K (Figure 4). Type I isotherms are obtained for the three gases, both on the monolith as the material in powder

form. The isotherms were fitted with the Langmuir and Sips isotherm (See SI, Figure S1). The best fit was obtained using the Sips equation, which is the one shown in Figure 4. Parameters obtained from fitting with Sips isotherm model are provided in Table 2. The presence of binder in the monolith reduces the capacity of the material to a comparable extent for N_2 and CH_4 as compared to the parent ZSM-5 zeolite (Table 2). This reduction of around 35% is in line with the amount of binder present, the reduction of adsorbed CO_2 on the other hand is only 10%, meaning the binders also adsorb a significant amount of CO_2. At 30 bar (almost saturation), the CO_2 capacity of the ZSM-5 monolith equals about 2 mmol/g; at a pressure of 0.1 bar (typical pressure of CO_2 in flue gas), CO_2 capacity equals 0.8 mmol/g. At 302 K, the Langmuir constant of CO_2 is 4 time larger than that of CH_4, which in turn is 3 times larger than that of N_2.

Isotherms were measured at four different temperatures (283K, 291K, 302K and 309K) for the monolithic structure (400µm fibers), to determine isosteric heats of adsorption. The Clausius-Clapeyron equation was applied on the fitted Sips isotherms to obtain heats of adsorption as a function of amount adsorbed (see SI, Figure S2-S4). At low degree of pore filling, the adsorption enthalpy of CO_2 is significantly larger than that of CH_4 and N_2 and reaches a value of 43 kJ/mol, but decreases rapidly with increasing amount adsorbed to a value of about 34 kJ/mol (Figure 5). On average, the adsorption enthalpy of CH_4 equals about 31-32 kJ/mol, while N_2 shows an adsorption enthalpy of 25-26 kJ/mol. Literature values (on a comparable H-ZSM-5, Si/Al: 30) for the heat of adsorption of CO_2, determined with different methods like inverse pulse GC, variable-temperature IR or calorimetry, vary from 28 kJ/mol to 34 kJ/mol[30-32]. For CH_4 and N_2, adsorption enthalpies of 25-28 kJ/mol[33] and 20 kJ/mol[30] respectively are reported based on calorimetry. Although the values we obtained tend to be higher than those found in literature, they show the same trend with N_2 having

the lowest heat of adsorption, followed by CH_4 and then finally CO_2. The higher heats of adsorption can be attributed to a partial exchange of -H atoms with cations present in the binder (a decrease of 31.6 % in acid sites per Å² was measured). The presence of cations would result in higher heats of adsorption as compared to the acid H-ZSM-5 zeolite. Based on the differences in Langmuir constants and heats of adsorption between CO_2 and the other gases, it could be expected that the 3DFD-printed monolithic ZSM-5 structure might allow separating CO_2 from nitrogen or methane.

Separation on both the 900 µm and 400 µm fiber monolith was studied (the 400 µm in lesser extent). Separating CO_2 from a gas stream containing various amounts of CH_4 or N_2 was studied via breakthrough measurements on the 900 µm monolith (Figure 6 A and B). On the 400 µm monolith only N_2/CO_2 separation was studied (Figure 6 C and D). Figure 6 represents the breakthrough profiles of CO_2-N_2 or CO_2-CH_4 gas mixtures containing 10 mole% CO_2 and 90 mole% N_2 or CH_4 and an equimolar mixture. On the 900 µm monolith, a very good separation is achieved for both gas mixtures. In accordance with isotherms, N_2 has the shortest breakthrough time and elutes almost immediately from the monolith, with a sharp breakthrough profile. CH_4 is retained a little longer in the column, but both N_2 and CH_4 have much shorter breakthrough times as compared to CO_2, which is strongly adsorbed in the material. Roll-up is obtained for N_2 and CH_4, showing that these weakly adsorbed components are displaced from the pores of the adsorbent by adsorbing CO_2 molecules. Similar experiments were performed for gas mixtures of different composition (mixtures containing 75% CO_2, 50% CO_2, 25% CO_2, 10% CO_2 and pure CO_2, N_2 and CH_4). Breakthrough profiles on the 400 µm monolith also indicate an excellent separation potential. The breakthrough times are shorter because the amount of monolith was much lower than for the 900 µm monolith. Figure 7 shows the binary adsorption isotherms obtained from these

data (900 µm monolith as well as the 400 µm monolith). As a result of the fast breakthrough of N_2 or CH_4 and their displacement by CO_2, the amounts adsorbed of both N_2 or CH_4 are low at all mixture compositions.

Regeneration of the 3DFD printed ZSM-5 monolith was performed by flushing the monolithic column with a 200 Nml/min He flow for one hour after a breakthrough experiment with an equimolar CO_2/N_2 mixture in isothermal conditions, at 303 K. Subsequently, separation of an equimolar N_2/CO_2 mixture was performed again. This procedure was repeated 3 times to check repeatability. Figure 8 (left) displays the different regeneration profiles. Whereas the N_2 concentration drops steeply and reaches a concentration below detection limit within 10 min., for CO_2 it takes a longer time to reach the base line, as expected. The corresponding breakthrough profiles, obtained after these regeneration treatments in isothermal conditions, are plotted in Figure 8 (right) and compared with an earlier obtained breakthrough profile where the monolith was regenerated by a thermal treatment at 393 K. From the perfect correspondence between the breakthrough-profiles obtained in different conditions, it is clear that full regeneration can be obtained without heating and merely flushing the column with an inert gas is sufficient to re-use the monolith. To verify if all CO_2 is removed from the column, a temperature profile after the one hour He flush was subjected to the monolith. The graphic result can be found in the supporting information (figure S5). It was found that only an extremely limited amount of CO_2 is released from the monolith and thus regeneration with only flushing is indeed sufficient. When the flushing time is reduced to only half an hour, it is noticed that the breakthrough time of CO_2 after such a regeneration is slightly decreased (from 3.4 to 3.3 minutes) (figure S6). If the regeneration of half an hour is repeated 3 times it is noticed that the breakthrough profiles afterwards

remain the same and CO_2 is not shifted any further. This means that for an optimal regeneration, 30 minutes is inadequate but it still gives very reasonable results.

Conclusion

The 3DFD printing method for making self-standing monolithic, zeolite-containing structures resulted in porous materials with a slightly decreased capacity as compared to the pure powder, which is mainly due to the binder (35wt%) used for making the monolithic structure. Nevertheless, the separation potential, assessed by means of breakthrough experiments, is excellent for CO_2/N_2 and CO_2/CH_4 separation. In all cases, CO_2 is the strongest adsorbing component. Full regeneration of the structure is achieved by flushing it with a Helium flow for one hour without the need to heat up the structure. This 3DFD printing method opens new possibilities for the tailor-made design of structured adsorbents with a possibility of improved heat transfer, optimized mass transfer and good separation performance.

Acknowledgements

S. Couck is grateful for the financial support of FWO Vlaanderen. The authors are grateful to FWO Vlaanderen for financial support for the G007113N project.

Table 1: Ar porosimetry data (BET surface area as calculated using the BET equation and pore volume using the DFT method.)

Material	Ar BET surface area (m^2/g)	Ar micropore volume (cc/g)[1]		Ar total pore volume (cc/g)[1]	Hg pore volume (cc/g)[3]	Volume of printed channels (cc/g)
		< 0.8 nm*	< 2 nm	< 100 nm	< 10 µm	
Powder	414	0.15	0.15	0.18	/	/
Monolith (900 µm)	261	0.09	0.10	0.29	0.51	1.91
Monolith (400 µm)	305	0.10	0.11	0.32	0.57	1.92

[1] Pore volume calculated with the DFT method

[2] Micropores attributed to pore system of ZSM-5 zeolite

[3] Pore volume from the high pressure measurement

Table 2: Parameters of isotherms fitted with Sips model (isotherms on monolith at 302 K) and average isosteric heats of adsorption of N_2, CH_4 and CO_2 measured on the monolith.

Component	q_{sat} (mmol/g)	K (1/bar)	n	$Q_{iso,average}$ (kJ/mol)
N_2 (on monolith)	1.08	0.19	1.00	25.3
CH_4 (on monolith)	1.41	0.57	0.98	31.7
CO_2 (on monolith)	2.39	2.25	0.48	36.1
N_2 (on powder)	1.70	0.16	1.03	/
CH_4 (on powder)	2.17	0.57	0.96	/
CO_2 (on powder)	2.67	6.38	0.67	/

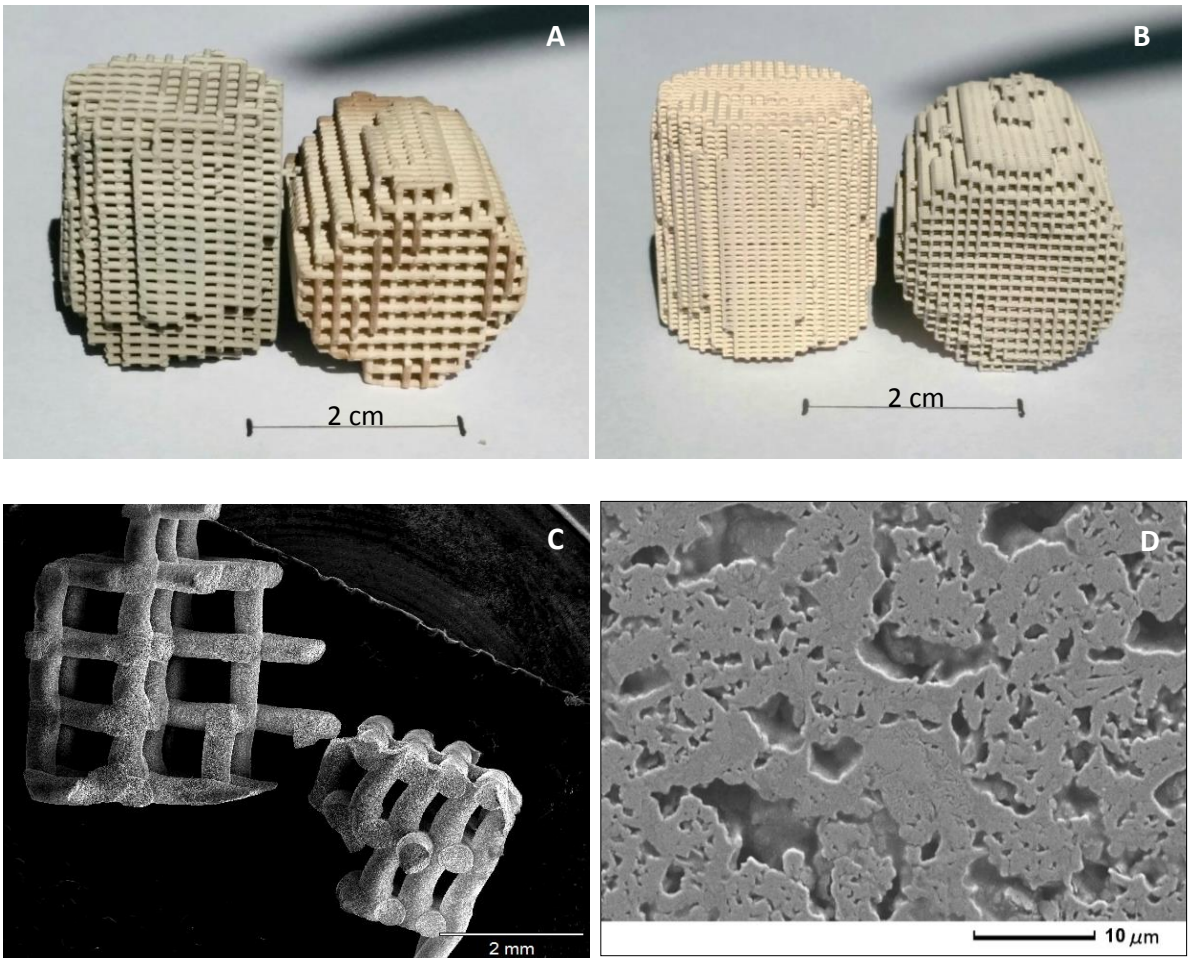

Figure 1: A: Picture of 900 µm monolith (scale = 2 cm); B: picture of 400 µm monolith (scale = 2 cm); C: SEM picture of a 1-1, 400µm fibre monolithic structure (scale = 2mm; left: top view; right: side view); D: zoom-in SEM picture of a 400µm fiber (scale = 10 µm).

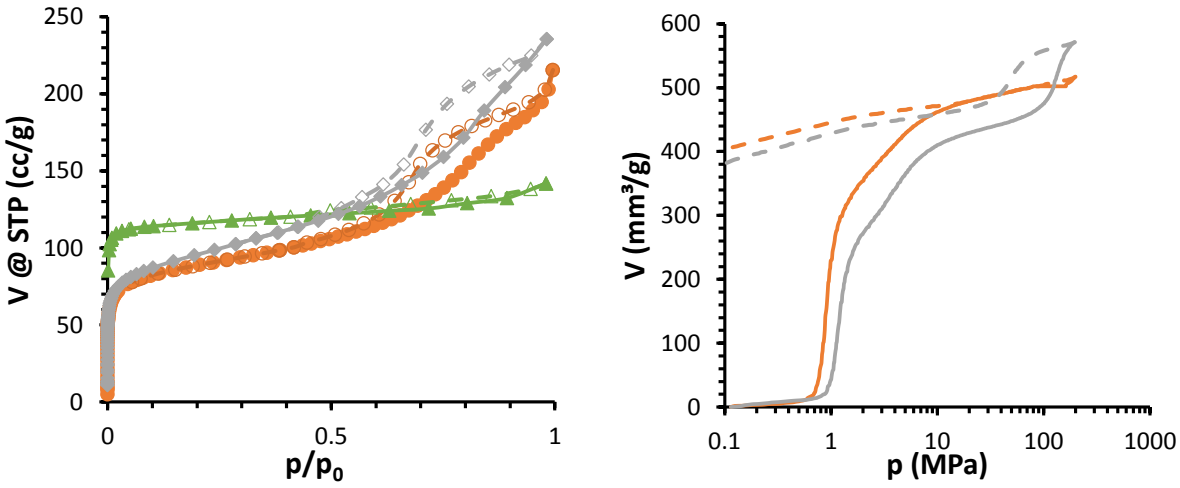

Figure 2: Left: Argon isotherms at 87K of powder H-ZSM-5 and the 3DFD-printed monolithic ZSM-5 structure (400 µm and 900 µm). Right: Hg porosimetry on both 3DFD printed monoliths. 900 µm monolithic structure: circles (orange); 400 µm monolithic structure: diamonds (gray); powder: triangles (green); closed symbols: adsorption; open symbols: desorption.

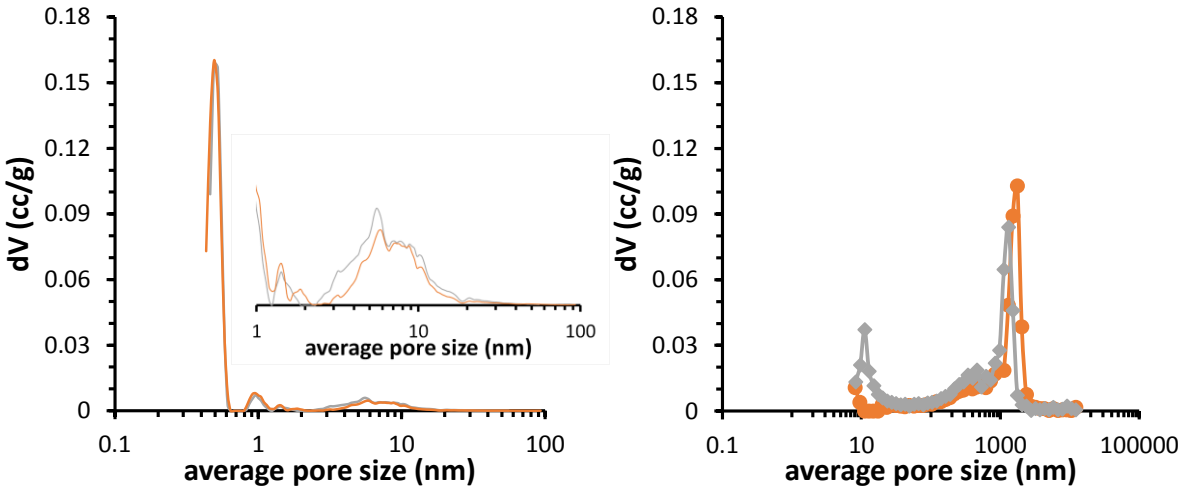

Figure 3: Pore size distribution. Left: as obtained from Ar porosimetry with a zoom-in on the larger pores. Right: as obtained from Hg porosimetry. Grey for 400 µm monolith; orange for 900 µm monolith.

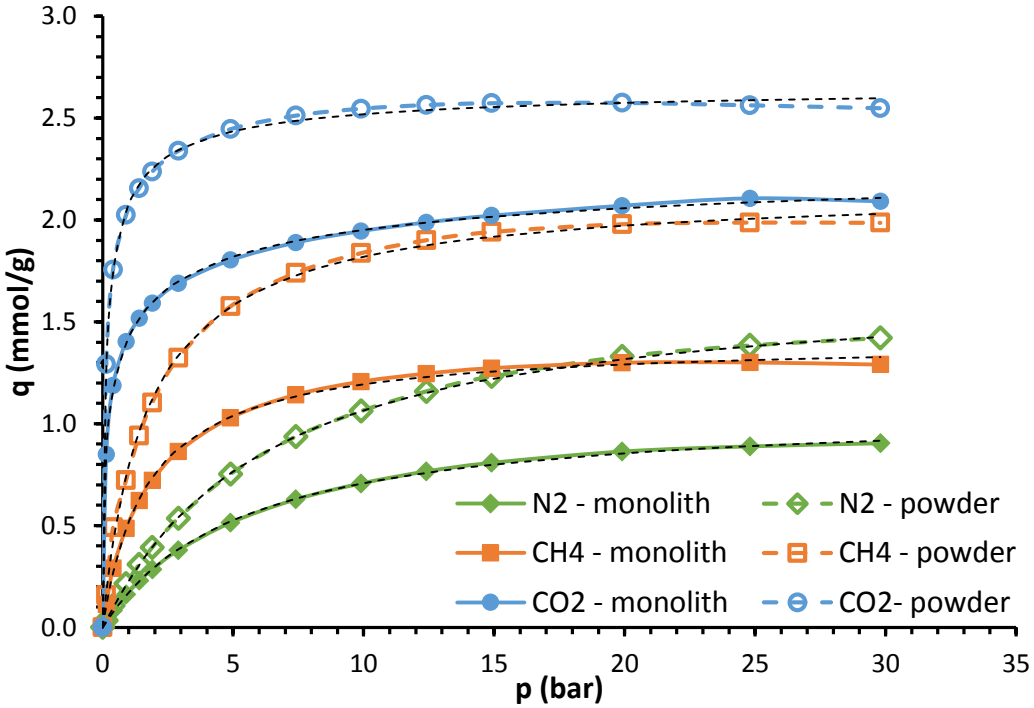

Figure 4: Adsorption isotherms of N_2, CH_4 and CO_2 on H-ZSM-5 powder and monolith (with 400 µm fibers), recorded at 302K. Black dotted lines represent the isotherm fitted with the Sipps isotherm model.

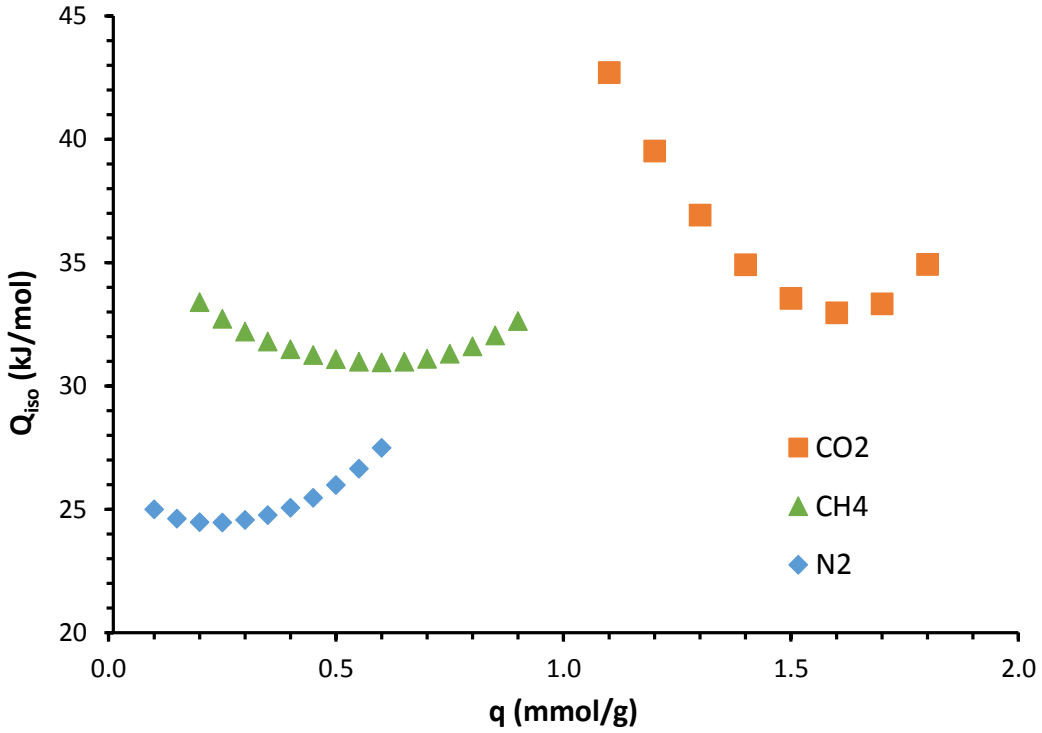

Figure 5: Isosteric heats of adsorption in function of loading for N_2, CH_4 and CO_2 on monolithic ZSM-5 structure (400µm fibre).

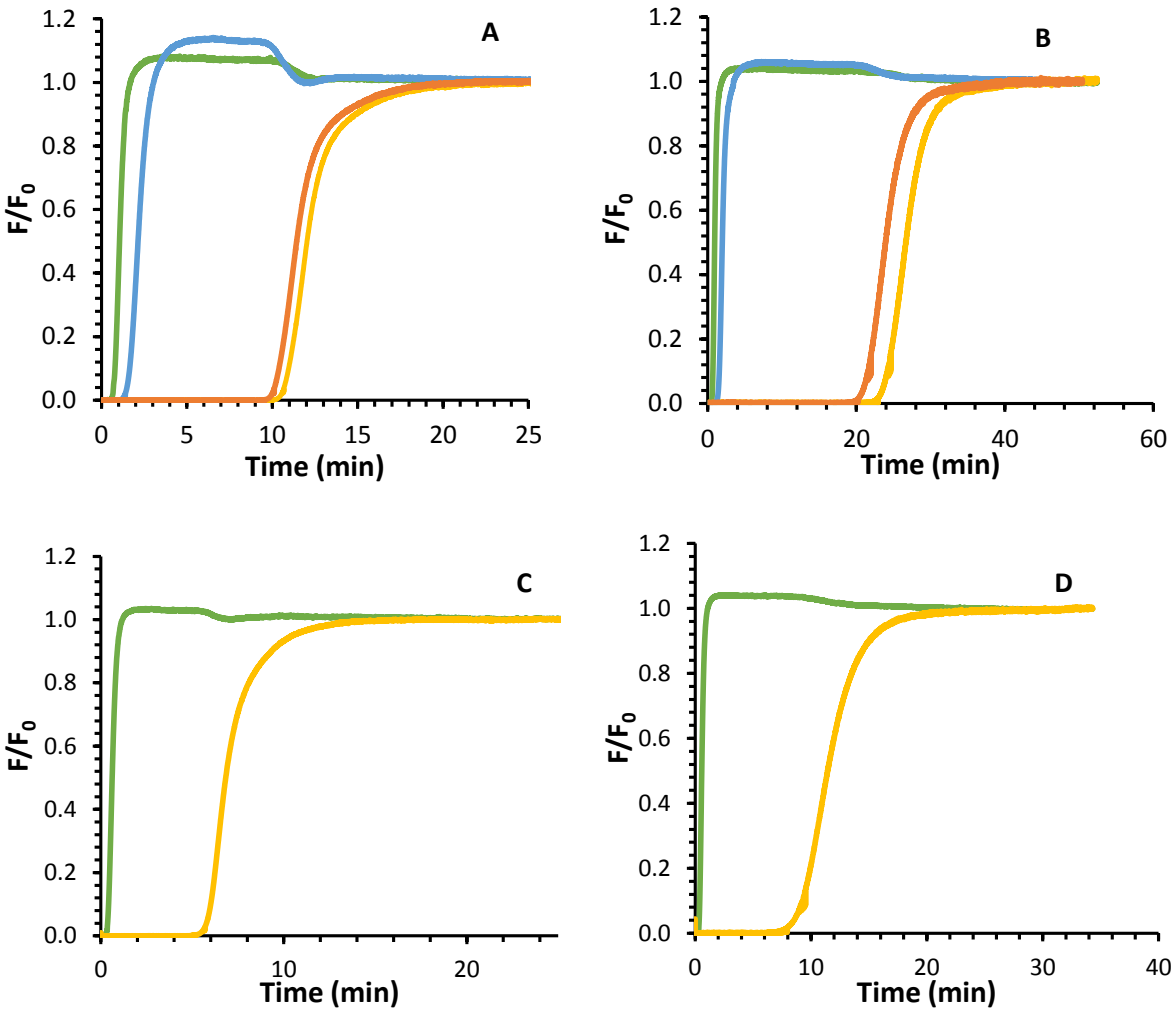

Figure 6: A: breakthrough profile of an equimolar N_2 or CH_4 with CO_2 mixture and B: a 90 mole% N_2 or CH_4 and 10 mole% CO_2 mixture, obtained on 3DFD-printed ZSM-5 monolith with 900 µm fibres at 303K. The volumetric flow rate of CO_2 and CH_4 or N_2 was equal to 50 Nml/min and diluted with a He flow of 150 Nml/min. C: breakthrough profile of an equimolar N_2/CO_2 mixture and D: a 90 mole% N_2 and 10 mole% CO_2 mixture, obtained on 3DFD-printed ZSM-5 monolith with 400µm fibres at 303K. The volumetric flow rate of CO_2 and N_2 was equal to 50 Nml/min and diluted with a He flow of 150 Nml/min. (Green = N_2; yellow= CO_2 corresponding with N_2; blue = CH_4; orange = CO_2 corresponding with CH_4).

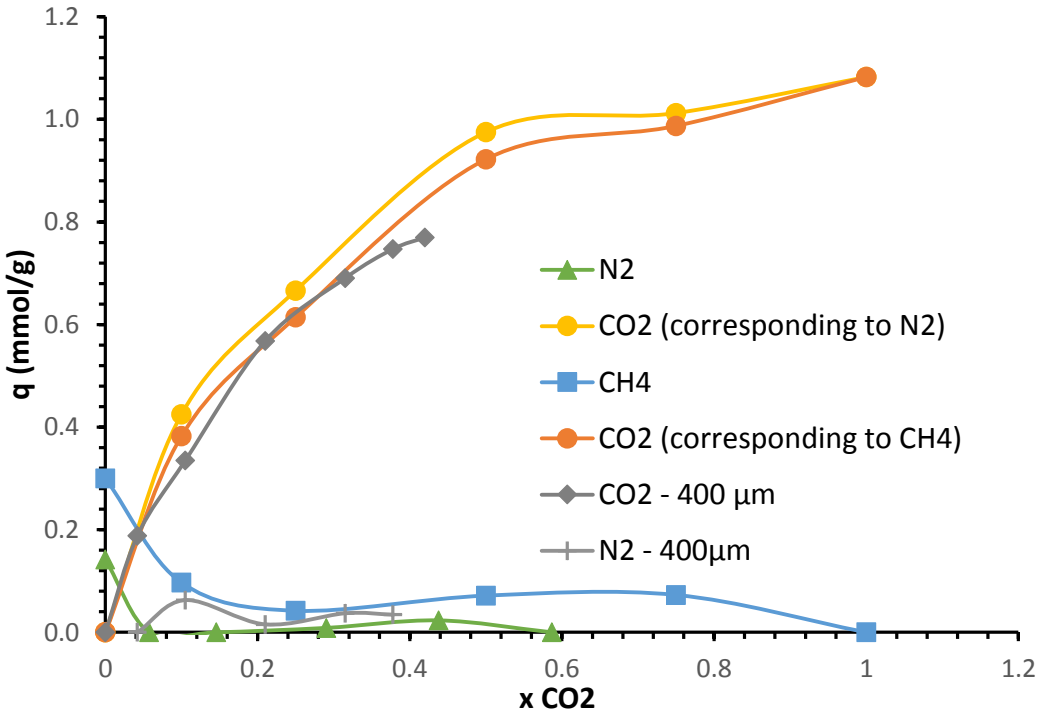

Figure 7: Breakthrough results plotted as capacity in function of CO_2 mole fraction.

Breakthrough data was collected at a total pressure of around 2.3 bar, a mixture flow rate of 50 Nml/min and 150 Nml/min He dilution (for the 900 µm monolith). For the 400 µm monolith, total pressure was 2.1 bar and mixture flow rate was 40 Nml/min with a 160 Nml/min He dilution flow. Lines are guidelines for the eye.

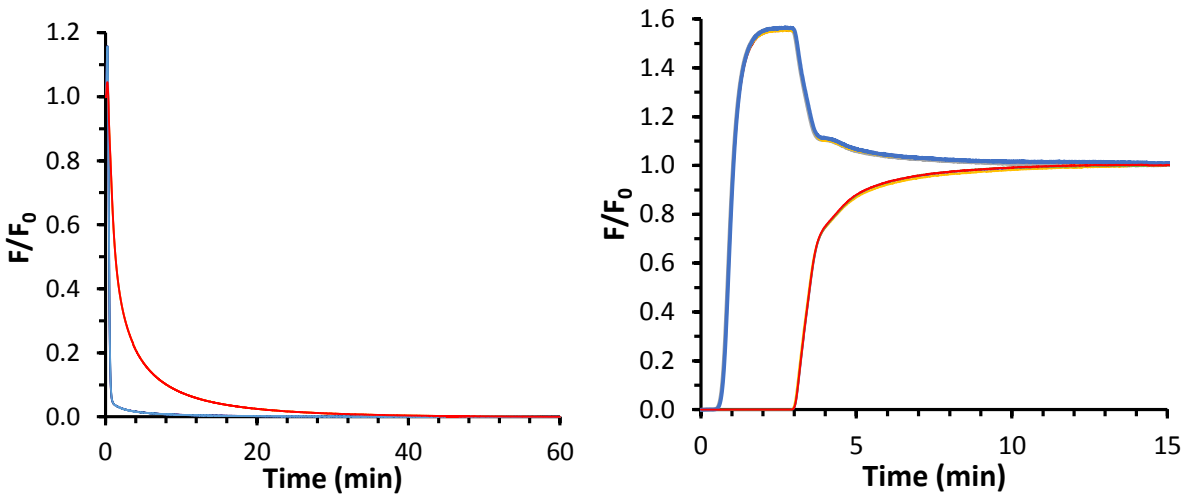

Figure 8: Left: desorption profiles obtained by flushing the 3DFD-printed ZSM-5 monolith with 200 Nml/min He at 303K (three successive regenerations, profiles overlapping). Right: breakthrough profiles in cyclic experiments with isothermal regeneration (using conditions of Fig. 8, left), measured at 303K with an equimolar N_2/CO_2 mixture at 200 Nml/min undiluted total gas flow (one profile obtained after thermal regeneration; three profiles after isothermal regeneration, profiles overlapping). As each successive breakthrough or desorption profile coincide with each other, no difference are visible in these graphs. Blue profile is N_2, red profile is CO_2.

References

[1] J. Janchen, T.H. Herzog, K. Gleichmann, B. Unger, A. Brandt, G. Fischer, H. Richter, Performance of an open thermal adsorption storage system with Linde type A zeolites: Beads versus honeycombs, Microporous and Mesoporous Materials, 207 (2015) 179-184.

[2] J.A.C. Silva, A.F. Cunha, K. Schumann, A.E. Rodrigues, Binary adsorption of CO2/CH4 in binderless beads of 13X zeolite, Microporous and Mesoporous Materials, 187 (2014) 100-107.

[3] D. Mehlhorn, R. Valiullin, J. Karger, K. Schumann, A. Brandt, B. Unger, Transport enhancement in binderless zeolite X- and A-type molecular sieves revealed by PFG NMR diffusometry, Microporous and Mesoporous Materials, 188 (2014) 126-132.

[4] F. Akhtar, L. Andersson, S. Ogunwumi, N. Hedin, L. Bergstrom, Structuring adsorbents and catalysts by processing of porous powders, Journal of the European Ceramic Society, 34 (2014) 1643-1666.

[5] F. Rezaei, P. Webley, Structured adsorbents in gas separation processes, Separation and Purification Technology, 70 (2010) 243-256.

[6] A. Mosca, J. Hedlund, P.A. Webley, M. Grahn, F. Rezaei, Structured zeolite NaX coatings on ceramic cordierite monolith supports for PSA applications, Microporous and Mesoporous Materials, 130 (2010) 38-48.

[7] T.A. Nijhuis, M.T. Kreutzer, A.C.J. Romijn, F. Kapteijn, J.A. Moulijn, Monolithic catalysts as efficient three-phase reactors, Chemical Engineering Science, 56 (2001) 823-829.

[8] F. Kapteijn, R.M. de Deugd, J.A. Moulijn, Fischer-Tropsch synthesis using monolithic catalysts, Catalysis Today, 105 (2005) 350-356.

[9] A. Cybulski, J.A. Moulijn, MONOLITHS IN HETEROGENEOUS CATALYSIS, Catalysis Reviews-Science and Engineering, 36 (1994) 179-270.

[10] K.K. Unger, R. Skudas, M.M. Schulte, Particle packed columns and monolithic columns in high-performance liquid chromatography-comparison and critical appraisal, Journal of Chromatography A, 1184 (2008) 393-415.

[11] P. Avila, M. Montes, E.E. Miro, Monolithic reactors for environmental applications - A review on preparation technologies, Chemical Engineering Journal, 109 (2005) 11-36.

[12] F. Rezaei, A. Mosca, P. Webley, J. Hedlund, P. Xiao, Comparison of Traditional and Structured Adsorbents for CO2 Separation by Vacuum-Swing Adsorption, Industrial & Engineering Chemistry Research, 49 (2010) 4832-4841.

[13] F.A. Hasan, P. Xiao, R.K. Singh, P.A. Webley, Zeolite monoliths with hierarchical designed pore network structure: Synthesis and performance, Chemical Engineering Journal, 223 (2013) 48-58.

[14] C.A. Grande, S. Cavenati, P. Barcia, J. Hammer, H.G. Fritz, A.E. Rodrigues, Adsorption of propane and propylene in zeolite 4A honeycomb monolith, Chemical Engineering Science, 61 (2006) 3053-3067.

[15] A. Aranzabal, D. Iturbe, M. Romero-Saez, M.P. Gonzalez-Marcos, J.R. Gonzalez-Velasco, J.A. Gonzalez-Marcos, Optimization of process parameters on the extrusion of honeycomb shaped monolith of H-ZSM-5 zeolite, Chemical Engineering Journal, 162 (2010) 415-423.

[16] M. Yates, J. Blanco, P. Avila, M.P. Martin, Honeycomb monoliths of activated carbons for effluent gas purification, Microporous and Mesoporous Materials, 37 (2000) 201-208.

[17] R.P.P.L. Ribeiro, T.P. Sauer, F.V. Lopes, R.F. Moreira, C.A. Grande, A.E. Rodrigues, Adsorption of CO2, CH4, and N-2 in Activated Carbon Honeycomb Monolith, Journal of Chemical and Engineering Data, 53 (2008) 2311-2317.

[18] L. Liu, Z. Liu, J. Yang, Z. Huang, Z. Liu, Effect of preparation conditions on the properties of a coal-derived activated carbon honeycomb monolith, Carbon, 45 (2007) 2836-2842.

[19] W.Y. Hong, S.P. Perera, A.D. Burrows, Manufacturing of metal-organic framework monoliths and their application in CO2 adsorption, Microporous and Mesoporous Materials, 214 (2015) 149-155.

[20] F. Rezaei, P. Webley, Optimum structured adsorbents for gas separation processes, Chemical Engineering Science, 64 (2009) 5182-5191.

[21] J.N. Stuecker, J.E. Miller, R.E. Ferrizz, J.E. Mudd, J. Cesarano, Advanced support structures for enhanced catalytic activity, Industrial & Engineering Chemistry Research, 43 (2004) 51-55.

[22] R.M. Ferrizz, J.N. Stuecker, J. Cesarano, J.E. Miller, Monolithic supports with unique geometries and enhanced mass transfer, Industrial & Engineering Chemistry Research, 44 (2005) 302-308.

[23] J.A. Lewis, J.E. Smay, J. Stuecker, J. Cesarano, III, Direct ink writing of three-dimensional ceramic structures, Journal of the American Ceramic Society, 89 (2006) 3599-3609.

[24] J. Van Noyen, A. De Wilde, M. Schroeven, S. Mullens, J. Luyten, Ceramic Processing Techniques for Catalyst Design: Formation, Properties, and Catalytic Example of ZSM-5 on 3-Dimensional Fiber Deposition Support Structures, International Journal of Applied Ceramic Technology, 9 (2012) 902-910.

[25] M. Rombouts, S. Mullens, J. Luyten, P. Nuyts, M. Schroeven, The production of Ti-6Al-4V parts with controlled porous architecture by three-dimensional fiber deposition, Innovative Developments in Design and Manufacturing: Advanced Research in Virtual and Rapid Prototyping, (2010) 453-457.

[26] M. Thommes, Physical Adsorption Characterization of Nanoporous Materials, Chemie Ingenieur Technik, 82 (2010) 1059-1073.

[27] M. Thommes, K.A. Cychosz, Physical adsorption characterization of nanoporous materials: progress and challenges, Adsorption-Journal of the International Adsorption Society, 20 (2014) 233-250.

[28] S. Couck, E. Gobechiya, C.E.A. Kirschhock, P. Serra-Crespo, J. Juan-Alcaniz, A.M. Joaristi, E. Stavitski, J. Gascon, F. Kapteijn, G.V. Baron, J.F.M. Denayer, Adsorption and Separation of Light Gases on an Amino-Functionalized Metal-Organic Framework: An Adsorption and In Situ XRD Study, Chemsuschem, 5 (2012) 740-750.
[29] S.A. Peter, G.V. Baron, J. Gascon, F. Kapteijn, J.F.M. Denayer, Dynamic desorption of CO2 and CH4 from amino-MIL-53(Al) adsorbent, Adsorption-Journal of the International Adsorption Society, 19 (2013) 1235-1244.
[30] J.A. Dunne, M. Rao, S. Sircar, R.J. Gorte, A.L. Myers, Calorimetric heats of adsorption and adsorption isotherms .2. O-2, N-2, Ar, CO2, CH4, C2H6, and SF6 on NaX, H-ZSM-5, and Na-ZSM-5 zeolites, Langmuir, 12 (1996) 5896-5904.
[31] P.J.E. Harlick, F.H. Tezel, An experimental adsorbent screening study for CO2 removal from N-2, Microporous and Mesoporous Materials, 76 (2004) 71-79.
[32] M. Armandi, E. Garrone, C.O. Arean, B. Bonelli, Thermodynamics of Carbon Dioxide Asdorption on the Protonic Zeolite H-ZSM-5, Chemphyschem, 10 (2009) 3316-3319.
[33] H. Papp, W. Hinsen, N.T. Do, M. Baerns, THE ADSORPTION OF METHANE ON H-ZSM-5 ZEOLITE, Thermochimica Acta, 82 (1984) 137-148.